ORIGINAL ARTICLE

Discovery of an orally effective double-stapled peptide for reducing ovariectomy-induced bone loss in mice

Wei Cong[a,†], Huaxing Shen[a,†], Xiufei Liao[b,c,†], Mengjun Zheng[b], Xianglong Kong[a], Zhe Wang[d], Si Chen[a], Yulei Li[e,*], Honggang Hu[a,*], Xiang Li[b,*]

[a]School of Medicine Or Institute of Translational Medicine, Shanghai University, Shanghai 200444, China
[b]School of Pharmacy, Second Military Medical University, Shanghai 200433, China
[c]Tarim University, Xinjiang Uygur Autonomous Region, Alar City 843300, China
[d]Institute of Bioengineering, College of Chemical and Biological Engineering, Zhejiang University, Hangzhou 310027, China
[e]School of Pharmacy and Pharmaceutical Sciences & Institute of Materia Medica, Shandong First Medical University & Shandong Academy of Medical Sciences, NHC Key Laboratory of Biotechnology Drugs (Shandong Academy of Medical Sciences), Key Lab for Rare & Uncommon Diseases of Shandong Province, Jinan 250117, China

Abstract Stapled peptides with significantly enhanced pharmacological profiles have emerged as promising therapeutic molecules due to their remarkable resistance to proteolysis and performance to penetrate cells. The all-hydrocarbon peptide stapling technique has already widely adopted with great success, yielding numerous potent peptide-based molecules. Based on our prior efforts, we conceived and prepared a double-stapled peptide in this study, termed FRNC-1, which effectively attenuated the bone resorption capacity of mature osteoclasts *in vitro* through specific inhibition of phosphorylated GSK-3β. The double-stapled peptide FRNC-1 displayed notably improved helical contents and resistance to proteolysis than its linear form. Additionally, FRNC-1 effectively prevented osteoclast activation and improved bone density for ovariectomized (OVX) mice after intravenous injection and importantly, after oral (intragastric) administration. The double-stapled peptide FRNC-1 is the first orally effective peptide that has been validated to date as a therapeutic candidate for postmenopausal osteoporosis (PMOP).

*Corresponding author.
E-mail addresses: fengyunliyu@sina.com (Yulei Li), hhu66@shu.edu.cn (Honggang Hu), xiangli@smmu.edu.cn (Xiang Li).
†These authors made equal contributions to this work.

1. Introduction

Insufficient bone mineral density (BMD) and lack of quality of bone are hallmarks of osteoporosis, and the World Health Organization (WHO) has labeled it a "serious public-related concern"[1,2]. The pathophysiological basis of osteoporosis is the imbalance between bone resorption and formation regulated by osteoblasts and osteoclasts, respectively[3]. Currently, widely used anti-osteoporotic drugs, including bisphosphonate, function through inhibiting osteoclast differentiation; however, they exhibit serious side effects[4–6]. In contrast, targeted molecular therapy is a superior form of therapy, as it can target specific proteins or signaling pathways related to osteoclast and osteoblast differentiation, which promises to be one of the hot areas of research about osteoporosis.

Earlier research has demonstrated that the Akt/GSK-3β/NFATc1 is a negative regulatory signaling pathway in osteoclasts, in which Akt (protein kinase B) phosphorylates GSK-3β (glycogen synthase kinase-3β) and then the phosphorylated GSK-3β promotes NFATc1 (nuclear factor of activated T-cells cytoplasmic 1) mediated osteoclast differentiation[7,8]. Accordingly, selectively inhibiting phosphorylated GSK-3β (its inactive state) can negatively regulate osteoclasts. Indeed, in our previous work we modeled a linear peptide (FRATtide) generated from a GSK-3β binding protein and developed a sequence of stapled peptides that target phosphorylated GSK-3β. The observed bioactivity indicated that the stapled peptides, termed FRC-2 and FRN-2, demonstrated the most osteoporosis therapeutic potential[9].

Owing to their excellent selectivity and effectiveness with less side effects, peptide-based therapies have gained increased attention[10–12]. Therapeutic peptides are usually administered *via* injection due to their weak proteolytic stability and poor cellular permeability[13]. One exception is the recent discovery of the orally accessible molecule Semaglutide approved by US Food and Drug Administration (FDA) for the treatment of type II diabetes[14,15]. Numerous elaborate studies have been dedicated to efficiently improving the pharmaceutical properties of linear peptides, including the structure-based design of peptidomimetics and development of nano-technique-aided delivery systems[16–24]. Among them, stapled peptides, of which the side chains are covalently linked to display the stabilized helical conformation, are one kind of attractive peptidomimetics due to their enhanced membrane permeability and proteolytic stability[20]. To date, various peptide stapling techniques were developed, and the all-hydrocarbon peptide stapling approach, initiated by Verdine and colleagues[25], is perhaps the most well-known and has been utilized to the construction of numerous peptide inhibitors for therapeutic application[26–33]. All-hydrocarbon peptide stapling technique takes advantages of the Grubbs catalyst-mediated ring-closing metathesis (RCM) reaction in solid phase, and thus efficiently affords the stapled peptides with feasible purification procedure. Of note, inserting a single all-hydrocarbon "staple" within lengthy peptide sequences has to some extent failed to retain the secondary helical structure and effectively enhance the proteolytic stability of the peptide[34]. It is not surprisingly as introducing a short hydrocarbon staple into a lengthy peptide hard to influence the whole secondary structures of the peptides. As such, hydrocarbon double-stapling was proven to be capable of improving the pharmacokinetic behavior of lengthy peptides. For example, a 36-amino acid lengthy HIV fusion inhibitor peptide was optimized *via* peptide double-stapling, and the resultant derivative exhibited striking proteolytic resistance and significantly improved pharmacokinetic features, including oral absorption[35].

According to previous results involving the structure−activity relationship (SAR) of the single-stapled peptide FRT0, herein we conceived and prepared a double-stapled peptide, termed FRNC-1, by replacing His200/Gln204 at the N-terminus and Ala216/Leu220 at the C-terminus with (S)-N-Fmoc-2-(4-pentenyl)alanine (S_5). Compared with the linear peptide, the resultant FRNC-1 peptide showed markedly enhanced helical content and proteolytic stability. FRNC-1 effectively attenuated the bone resorption capacity of mature osteoclasts *in vitro* through specific inhibition of phosphorylated GSK-3β. Importantly, FRNC-1 potently prevented osteoclast activity and decreased bone loss in ovariectomized (OVX) mice after intravenous injection and even after oral (intragastric) administration. To our knowledge, FRNC-1 has been identified as the first double-stapled, orally effective peptide therapy strategy for PMOP and disorders associated with osteoclastogenesis.

2. Results and discussion

2.1. Structure-based design and synthesis of double-stapled peptide

Discovered in *Xenopus* embryos, FRATtide is a 26 amino acid long peptide (from Asp198 to Arg223) consisting of two helical peptides with comparatively small lengths[36,37]. In our previous work, several stapled peptides were rationally designed by changing the noninteracting residues at the *i*, *i*+4 positions, and the sequences of FRN-2 and FRC-2 were indicated to be optimal. The corresponding residues replaced for stapling were His200/Gln204 at the N-terminus and Ala216/Leu220 at the C-terminus. In this research, we introduced double olefin-terminated S_5−S_5 amino acids and translated the lengthy linear peptide into the double-stapled peptide derivative FRNC-1 (Fig. 1A). The complete synthesis scheme is shown in Fig. 1B. Using rink amide resin as the solid phase support, the first half of the linear peptide until Gln205 was assembled with the aid of solid-phase peptide synthesis (SPPS), followed by the first RCM reaction in the presence of Grubbs' first-generation catalyst. Then, the remaining of the peptide sequence was assembled, and the second staple was introduced using the similar RCM procedure. Two repeated 2-h RCM reactions in 1,2-dichloroethane were carried out at a concentration of 10 mmol/L Grubbs' catalyst. The crude double-stapled peptide, cleaved using reagent B (88% trifluoroacetic acid (TFA), 5% H_2O, 5% phenol and 2% triisopropylsilane
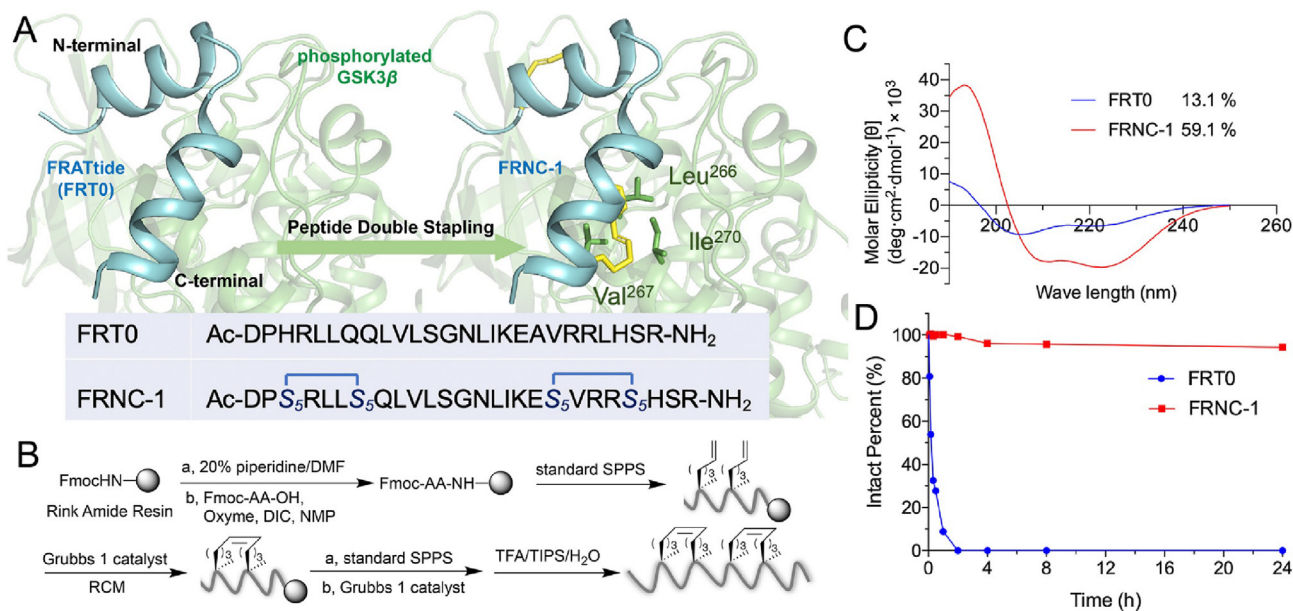
Figure 1 Design, synthesis and characterization of double-stapled peptide modeled after FRATide (FRT0). (A) FRT0 targeting phosphorylated GSK-3β was i, $i+4$ double-stapled by replacing His200/Gln204 at the N-terminus and Ala216/Leu220 at the C-terminus with S_5, thereby resulting in the FRNC-1 peptide. (B) Synthetic route of FRNC-1. (C) Circular dichroism spectra of FRT0 and FRNC-1. (D) The stability of stapled peptides to α-chymotrypsin was evaluated by monitoring the remaining peptide using analytical HPLC. The tests were conducted twice independently, and the consistent results were obtained. The reaction mixture contained 5 ng/mL of α-chymotrypsin and 100 μmol/L peptide in 50 mmol/L PBS (pH 7.4).

(TIPS)) from the resin, was purified by reversed-phase high-performance liquid chromatography (RP-HPLC) and verified by HPLC (>95%) and high-resolution mass spectrometry (HR-MS) (Supporting Information Figs. S1–S2). ESI-MS m/z of FRNC-1 was calculated for $C_{143}H_{246}N_{44}O_{35}$ 3139.8822 and found $[M + 2H]^{2+} = 1571.4453$, $[M + 3H]^{3+} = 1047.9661$, $[M + 4H]^{4+} = 786.2291$, $[M + 5H]^{5+} = 629.1858$, $[M + 6H]^{6+} = 524.4873$.

2.2. Helicity and proteolytic stability

Circular dichroism (CD) spectroscopy was applied to research how double-stapling affected the peptide's helicity. In this case we used phosphate buffer (PB) without sodium as the solution to perform the relevant experiments. As shown in Fig. 1C, FRNC-1 showed a notably higher helical content (59.1%) than its linear counterpart (13.1%). It should be noted that this double-stapled peptide displayed intermediate helicity between FRN-2 and FRC-2, whose helical contents were approximately 68% and 40%, respectively[9]. To determine the proteolytic resistance of the peptides, we subjected FRT0 and FRNC-1 to in vitro α-chymotrypsin digestion and monitored the degradation kinetics by HPLC. The linear peptide was rapidly cleared within 2 h, whereas no obvious change was observed for the double-stapled FRNC-1 peptide even after a 24 h degradation, demonstrating its superior proteolytic stability (Fig. 1D). Additionally, we have monitored the change of FRNC-1 in plasma and the concentration of peptide remained unchanged even over 48 h (Supporting Information Fig. S3). The results are similar to that of an HIV fusion inhibitor peptide, whereas the level of overall α-helicity did not explain the higher proteolytic resistance of doubly stapled peptides[35].

2.3. The double-stapled peptide inhibits osteoclastogenesis and bone resorption in vitro

Osteoblasts are primarily responsible for bone production and are derived from mesenchymal stem cells (MSCs), whereas osteoclasts are huge multinucleated cells whose major role is bone resorption. Osteoclasts are derived by bone marrow macrophages (BMMs) of the hematopoietic cell lineage[38,39]. Multiplex experiments were used in our study to verify the effects of the double-stapled peptide FRNC-1 on osteoblast and osteoclast function. The linear peptide control FRT0 had no obvious suppressive activities on the proliferation of BMMs and MSCs and stapled FRNC-1 had also slight inhibitory activity on BMM and MSC cell lines at concentrations up to 5 and 2.5 μmol/L, respectively (Fig. 2A, Supporting Information Fig. S4). Of note, FRNC-1 nearly killed all the BMM and MSC cells at the concentration of 10 μmol/L, showing an obviously enhanced cytotoxicity than the linear FRT0. More mutational analysis against FRNC-1 would be performed in our next experiments to further decrease the inhibitory activities on BMM and MSC cells. We next examined that whether FRNC-1 was capable of penetrating the cellular membrane. High content analysis of BMMs and the osteoclasts cells treated with 5 μmol/L fluorescein (FITC)-modified FRNC-1 revealed a diffused intracellular distribution of the peptide (Fig. 2B), confirming the capacity of FRNC-1 to penetrate cytomembrane. To understand the effect of FRNC-1 on osteoclast-related gene levels, we examined tartrate-resistant acid phosphatase (TRAP), Cathepsin K (CTSK), NFATc1, and matrix metalloproteinase 9 (MMP9) and found that all of these genes were considerably down-regulated under the effect of FRNC-1 (2.5 μmol/L), indicating that FRNC-1 played a favorable func-

tion in inhibiting osteoclast differentiation (Fig. 2C). Above results potentially validated that FRNC-1 could enter the cell and inhibit osteoclastogenesis at the safe concentration.

We next performed three independent experiments to confirm the potency of FRNC-1 peptide against osteoclastogenesis, including TRAP, bone resorption and F-actin. BMMs differentiated into mature osteoclasts under the interaction of macrophage-colony stimulating factor (M-CSF) and receptor activator of nuclear factor kappa-B ligand (RANKL). TRAP is usually used as an important marker to identify osteoclasts. The surrounding or cytoplasmic part of osteoclasts stained by TRAP appeared wine red. We added serial concentrations of FRNC-1 and FRT0 during M-CSF and RANKL-induced BMMs maturing into osteoclasts. Induced BMMs successfully differentiated from mononuclear macrophages into multinucleated osteoclasts without the addition of stapled peptides. These osteoclasts were stained wine red by TRAP. Nevertheless, this differentiation process was obviously inhibited by FRNC-1. Even at the lowest concentration of 0.625 µmol/L, significantly less area was stained fuchsia (Fig. 2D). In contrast, nearly no detectable decrease could be observed for the highest concentration (2.5 µmol/L) of FRT0 (Fig. 2E).

Osteoclasts can secrete acids, lysosomal enzymes and collagenases to dissolve substances in bone. Therefore, the bone resorption function of osteoclasts was detected using 96-well plates containing hydroxyapatite. In the control group, more than 85% of the area of hydroxyapatite with mature osteoclasts added was absorbed, appearing grayish-white, which fully demonstrated the function of osteoclasts. The bone resorption area of FRT0 group was similar to the control group, and it did not show inhibition of bone resorption by osteoclasts. The differences were that the amount of grayish-white area was reduced in the FRNC-1 groups, especially the high-dose group, where the grayish-white area was less than 60% (Fig. 2F–G). These results suggested that FRNC-1 could inhibit osteoclast bone resorption.

Differentiation of BMMs into osteoclasts was visualized by phalloidin staining for F-actin, and mature osteoclasts were vesicular and contained multiple nuclei. Actin is involved in the formation of the cytoskeleton and can be stained red by phalloidin. In relatively small mononuclear macrophages (blank group), actin was punctate, and the red dot corresponds to a blue nucleus (Hoechst 33342 staining). Osteoclasts in the control group were vesicular, and actin appeared as large red rings surrounding the cells. Each ring contained multiple blue nuclei. In the FRNC-1 groups, the decrease in large vesicular cells was particularly pronounced in the high-dose group and these results were statistically significant (Fig. 2H–I). The above results collectively indicated that the double-stapled peptide FRNC-1 exhibited excellent inhibitory activity against osteoclastogenesis and osteoclast resorption.

FRNC-1 showed potency in inhibiting osteoclast differentiation in previous experiments, and we further examined whether FRNC-1 would inhibit osteoblast differentiation to affect efficacy. Osteoblasts are differentiated by MSCs induced by L-ascorbic acid and β-glycerophosphate. During differentiation, alkaline phosphatase expression increased and mineralization formed calcium nodules, which were stained black and red by alkaline phosphatase and alizarin red S, respectively. In the osteoblast-induced differentiation assay, the control group was successfully stained black and red, indicating that MSCs had successfully differentiated into osteoblasts, while similar results to the control group were observed in the FRT0 and FRNC-1 treated groups (Supporting Information Fig. S5). Thus, with or without the addition of stapled peptides, there was no significant effect on the differentiation process of MSCs. Above

experimental results suggested that the double-stapled peptide inhibited not only the BMMs maturing into osteoclasts but also bone resorption by mature osteoclasts. Hence double-stapled FRNC-1 peptide has great application potential for the treatment of osteoporosis caused by bone loss.

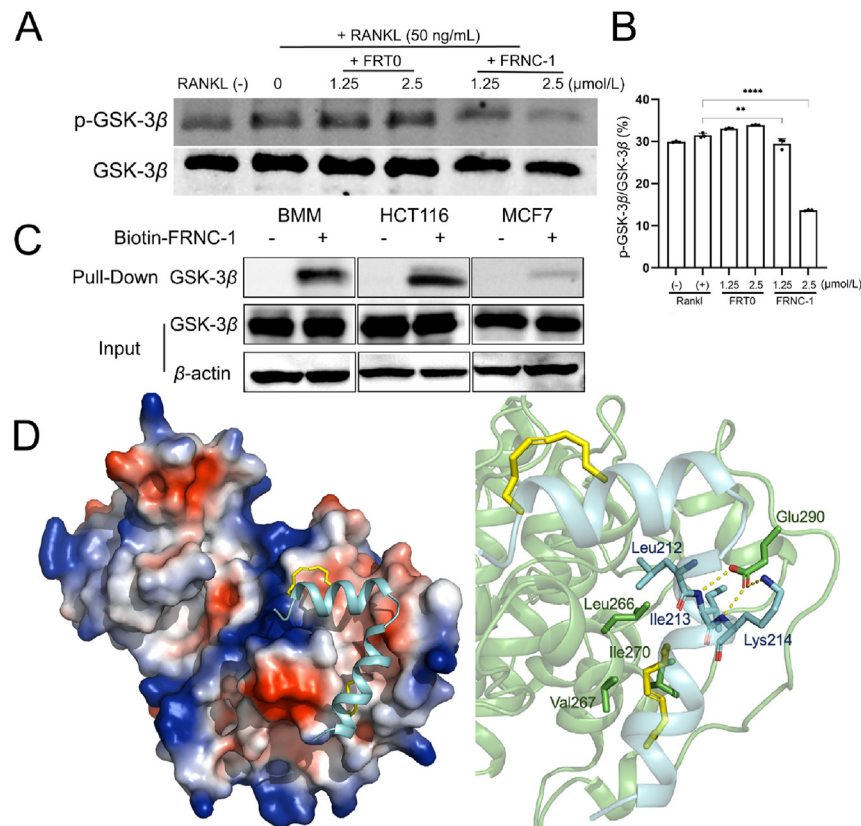### 2.4. The double-stapled peptide specifically targeted phosphorylated GSK-3β to impede osteoclastogenesis

In our previous work, we validated that the single-stapled peptide could target phosphorylated GSK-3β to inhibit osteoclastogenesis[9]. As such, we tested whether the double-stapled peptide FRNC-1 displayed a similar effect. As shown in Fig. 3A and B, dose-dependent downregulation of the level of phosphorylated GSK-3β was observed in the presence of FRNC-1, whereas no obvious change was observed in the group with the linear counterpart. Notably, the dose-dependent decrease in phosphorylated GSK-3β suggested that the specific inhibition of GSK-3β may be a mechanism triggered by FRNC-1 to inhibit osteoclastogenesis. We then examined whether the peptide interacted with GSK-3β by Pull-Down assay, and the results demonstrate that FRNC-1 and GSK-3β interacted strongly in BMMs and HCT116 cells (Fig. 3C). Next, we explored the binding mode of FRNC-1 with phosphorylated GSK-3β with the aid of structural modeling analysis. Not surprisingly, FRNC-1 could bind with the target protein in a similar way to the linear counterpart because of the high similarity of these two sequences (Fig. 3D). Three H-bonds could be formed between Ile213 and Lys214 of FRNC-1 with Glu290 of phosphorylated GSK-3β, similar to that found in the complex of FRT0 with the target protein[37]. Importantly, an extra hydrophobic interaction could be observed between the staple at the C-terminus of FRNC-1 and Val267 and Ile270 of the target protein. Such a phenomenon was seen in some cases[40], which probably conferred the potential for enhanced stapled peptides' affinity for target proteins. Together, the above results could explain the potential mechanism of the manner of action of the double-stapled peptide FRNC-1.

2.5. The double-stapled peptide prevented OVX-induced bone loss in vivo

OVX mice cam mimic osteoporosis in menopausal women[41]. The model was made by removing both ovaries from mice for assess the impact of FRNC-1 on osteoporosis. One week following surgery, mice received subcutaneous injections of FRNC-1 for seven weeks, three times each week. We set two doses of FRNC-1:2 mg/kg (milligrams per kilogram of body weight) and 5 mg/kg (Fig. 4A). When the experiment was over, the distal femur structure of mice was analyzed by using microcomputed tomography (micro-CT). The trabeculae under the growth plate were reconstructed by using software, and 3D reconstruction was performed. It was obvious from the pictures that both the number and volume of trabecular bone in the control group had decreased significantly. This appearance indicated that the OVX model was successfully established. In OVX mice treated with FRNC-1 (5 mg/kg), similar numbers and volumes of trabecular could be observed in the sham and treatment group (Fig. 4B). A series of parameters including percent bone volume BV/TV, bone surface density BS/TV, trabecular number (Tb.N), BMD, structure model index (SMI), trabecular thickness (Tb.Th), and trabecular separation (Tb.Sp) could be calculated according to microstructure of the trabecular bone. These are the key indicators required to determine the morphology spatial of trabecular bone. When bone catabolism
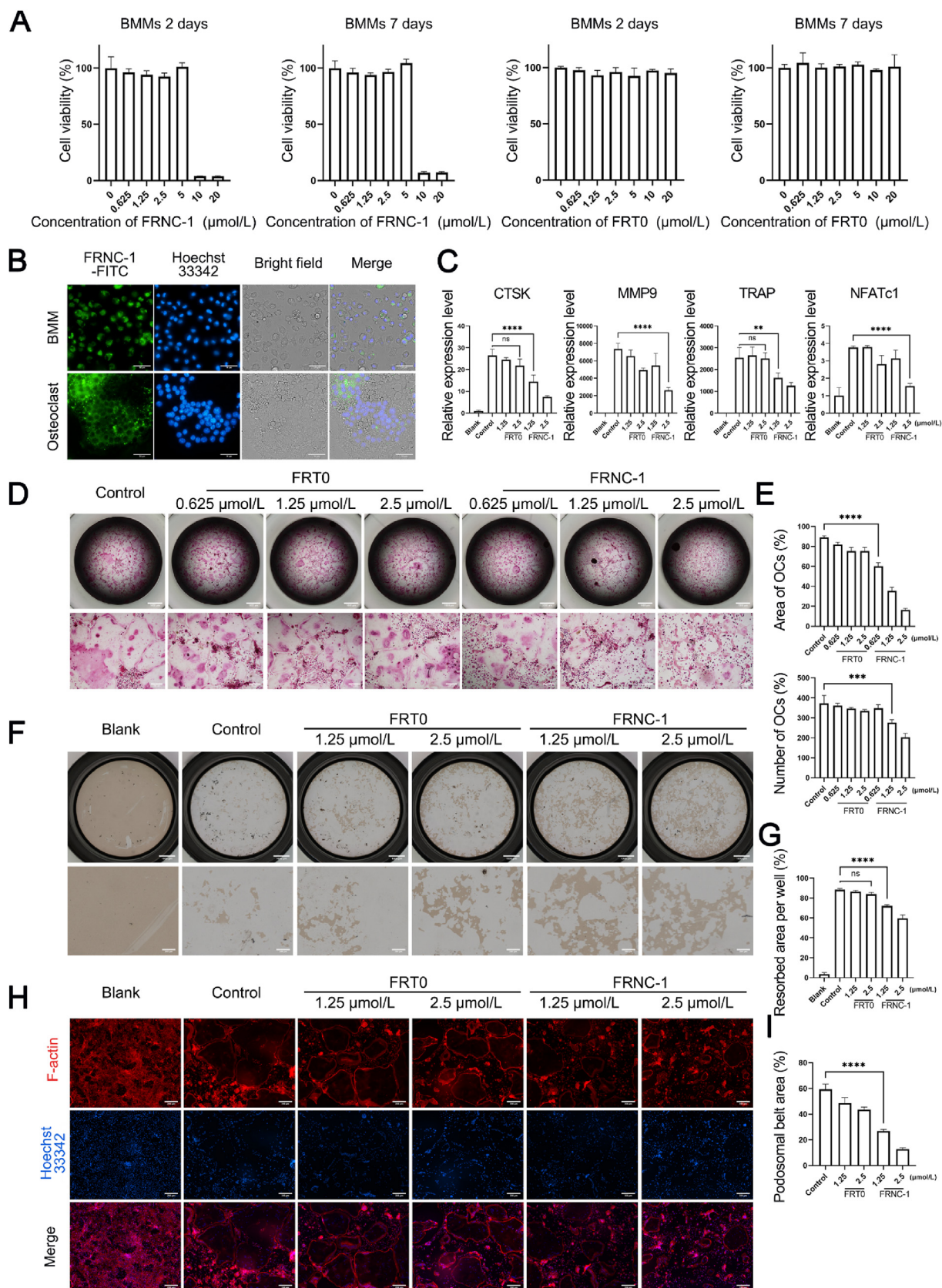
Figure 2 The double-stapled peptide exhibited excellent inhibitory activities against osteoclasts *in vitro*. (A) BMMs cells were treated with FRT0 and FRNC-1 for 2 or 7 days and tested for cytotoxicity using CCK-8 reagent. (B) FITC-modified FRNC-1 (green) was incubated with BMMs and osteoclasts for 6 h to detect drug permeability to cells. Cell nuclei (blue) were stained using Hoechst 33342 and high-content analysis system was used for photography. Scale bar = 50 μm. (C) FRNC-1 or FRT0 were added into osteoclast media for 7 days stimulation and qPCR
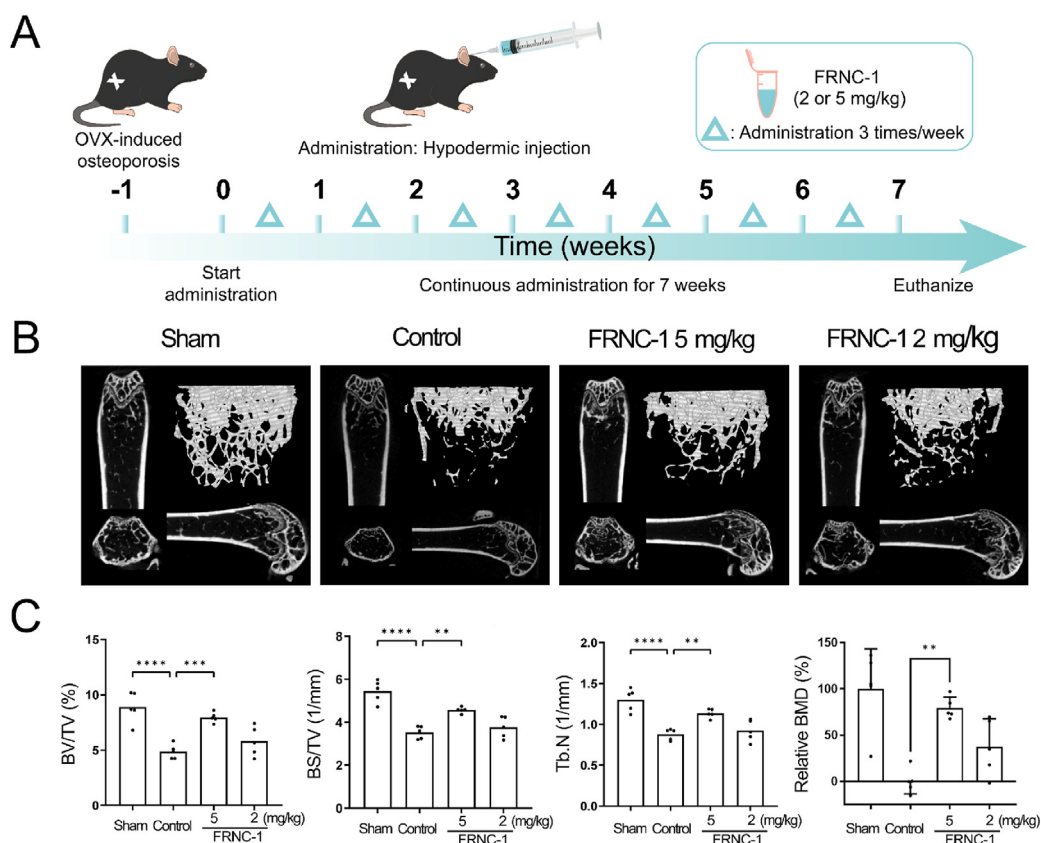
Figure 3 The double-stapled peptide FRNC-1 specifically targeted phosphorylated GSK-3β to impede osteoclastogenesis. (A) The expression of phosphorylated GSK-3β was dose-dependently suppressed by FRNC-1. BMMs were incubated using RANKL (50 ng/mL) for 1 h before being incubated using 1.25 or 2.5 μmol/L FRNC-1 or FRT0 for 24 h. (B) Quantification of phosphorylated GSK-3β levels according to the level of total GSK-3β using Image J software (**$P < 0.01$; ****$P < 0.0001$). Statistics are means $\pm$ SD, $n = 3$. (C) Pull-Down experiments verified the interaction between FRNC-1 and GSK-3β, especially in BMMs. (D) An overall view of the structural modeling of the stapled peptide FRNC-1 complexed with phosphorylated GSK-3β and the detailed analysis of the binding modes between FRNC-1 and the target protein. FRNC-1 is depicted as a cyan cartoon, and the hydrocarbon staples are depicted as yellow sticks. The key residues are depicted as sticks. The yellow dashes represent H-bonds.

exceeded bone anabolism, such as in osteoporosis, BV/TV, BS/TV, BMD, Tb.N and Tb.Th values declined and the Tb. Sp value rose. In our case, BV/TV, BS/TV, Tb.N, BMD and Tb.Th values of the mice were significantly growth when treated with FRNC-1 peptide (Fig. 4C, Supporting Information Fig. S6A). There existed no obvious difference between sham, control and peptide groups for additional SMI and Tb. Sp parameters (Fig. S6B−C). H&E staining analysis of visceral pathological sections showed no significant pathological changes in sham, control and FRNC-1 group (Supporting Information Fig. S7). The experimental results showed that osteoporosis in mice was effectively significantly remedied by subcutaneous injection of FRNC-1.

Due to poor stability, most peptides can be destroyed when exposed to digestive juices in the gastrointestinal tract. Therefore,

their clinical applications are limited. Consequently, very few peptide drugs currently on the market are orally administered. To broaden the clinical application value of this double-stapled peptide, we considered validating its anti-osteoporotic efficacy in mice after oral administration. To ensure that each mouse received the same drug dose, intragastric injection was used in our study. One week before dosing, mice were subjected to OVX surgery. After successful establishment of the model, mice began to receive intragastric FRNC-1 and FRT0 for 8 weeks. The frequency was the same as before: 3 times a week (Fig. 5A). Considering that the drug might be destroyed by digestive juice when passing through the gastrointestinal tract, the high-dose group was administered as 10 mg/kg. FRT0 was applied as a control drug to test the effectiveness of the double-stapling modification

was used to quantify the expression of CTSK, MMP9, TRAP, and NFATc1. (D) The inhibitory effects of different concentrations of FRT0 and FRNC-1 (0, 0.625, 1.25 and 2.5 μmol/L) on BMM formation were tested by TRAP staining analysis. The upper scale bar $=$ 1000 μm, the lower scale bar $=$ 200 μm. (E) The TRAP$^+$ areas and quantities after treatment with FRNC-1 or FRT0 during osteoclastogenesis. (F) FRT0 and FRNC-1 (1.25 and 2.5 μmol/L) were added to osteoclasts activated with RANKL, and the growth state of the osteoclasts was viewed by the microscope. The upper scale bar $=$ 1000 μm, the lower scale bar $=$ 200 μm. (G) Bone resorption rate statistics. (H) The first row of images showed phalloidin-stained actin as red bands, the middle row of images showed DAPI-stained nuclei in blue, and the bottom row the merge of the two images. Scale bar $=$ 200 μm. (I) Area statistics calculation of the F-actin ring in panel H. P-values were calculated using the t-test (**$P < 0.01$; ***$P < 0.001$; ****$P < 0.0001$). Statistics are expressed as means $\pm$ SD, $n = 3$.

Figure 4 Hypodermic injection of the double-stapled peptide FRNC-1 effectively prevented OVX-induced bone loss *in vivo*. (A) The OVX mice experimental design and therapeutic scheme of FRNC-1. OVX mice were treated with FRNC-1 or FRT0 by hypodermic injection according to the following schedule: 3 doses of 2 or 5 mg/kg weekly for 49 days. (B) High-resolution micro-CT scans were performed on the femurs of each mouse. (C) Microstructural indicators including BV/TV, BS/TV, Tb.N and BMD were quantitively analyzed (**$P < 0.01$; ***$P < 0.001$ ****$P < 0.0001$). Statistics were expressed as means $\pm$ SD, $n = 5$.

approach. At the end of treatment, femurs were reconstructed and analyzed using the same instruments and software. The statistical data of the sham and the control group were similar to those of previous experiments, indicating that the osteoporosis model was successful. Micro-CT images in the FRNC-1 high-dose group gave us the encouraging results of a notable increase in both the number and volume of trabecular bone (Fig. 5B). This suggested that FRNC-1 withstood the destruction of digestive juices and was able to ameliorate osteoporosis symptoms in OVX mice. In contrast, the mice in the low-dose FRNC-1 and the FRT0 group were ineffectively treated. Furthermore, statistically significant trabecular bone spatial morphology and structural indicators, including BV/TV, BS/TV and Tb.N, provided confidence in the FRNC-1 high-dose group (Fig. 5C). Similar as that in the sub-cutaneous injection experiment, no remarkable change was observed for another Tb.Th, SMI and Tb. Sp values (Supporting Information Fig. S8). These results indicated that mice treated with the high dose of FRNC-1 did not develop or had only mild osteoporosis.

In order to observe the metabolism of FRNC-1 in the blood of mice, we analyzed the change of drug concentration in serum after multiple doses by different routes of administration. Obvious blood peptide concentration of FRNC-1 was detected in intragastric route, indicating that the peptide could enter the plasma and exert anti-osteoporotic effects, although the concentration was slightly lower than that in hypodermic injection (Supporting Information Table S1). In summary, the double-stapled peptide

FRNC-1 was proven in two kinds of *in vivo* experiments to be capable of treating bone loss caused by osteoporosis. Notably, the potential therapeutic effect of FRNC-1 remained even when orally administered.

3. Conclusions

Osteoporosis has been identified as a public health threat, and effective treatment remains challenging. Notable peptide examples, such as teriparatide, have been proven to be capable of stimulating bone remodeling and increasing bone mass and have thus been approved by the FDA as bone-building agents. However, conventional peptide drugs should be administered by injection, which restricts their further applications. All-hydrocarbon peptide stapling, featuring RCM-mediated side chain to side chain cyclization, has been utilized for protein−protein interactions to afford various peptidomimetics with notably enhanced proteolytic stability and cellular uptake. Based on FRT0, a 26 amino acid long peptide that can bind with phosphorylated GSK-3β, we designed a double-stapled peptide, termed FRNC-1, by replacing His200/Gln204 at the N-terminus and Ala216/Leu220 at the C-terminus with S_5 amino acids. FRNC-1 exhibited significantly improved helical contents and proteolytic stability than its linear form. More importantly, the double-stapled peptide FRNC-1 effectively suppressed osteoclast and reduced bone loss *in vitro* and in OVX mice after both intravenous injection and oral administration. The double-stapled peptide FRNC-1 was the first orally effective
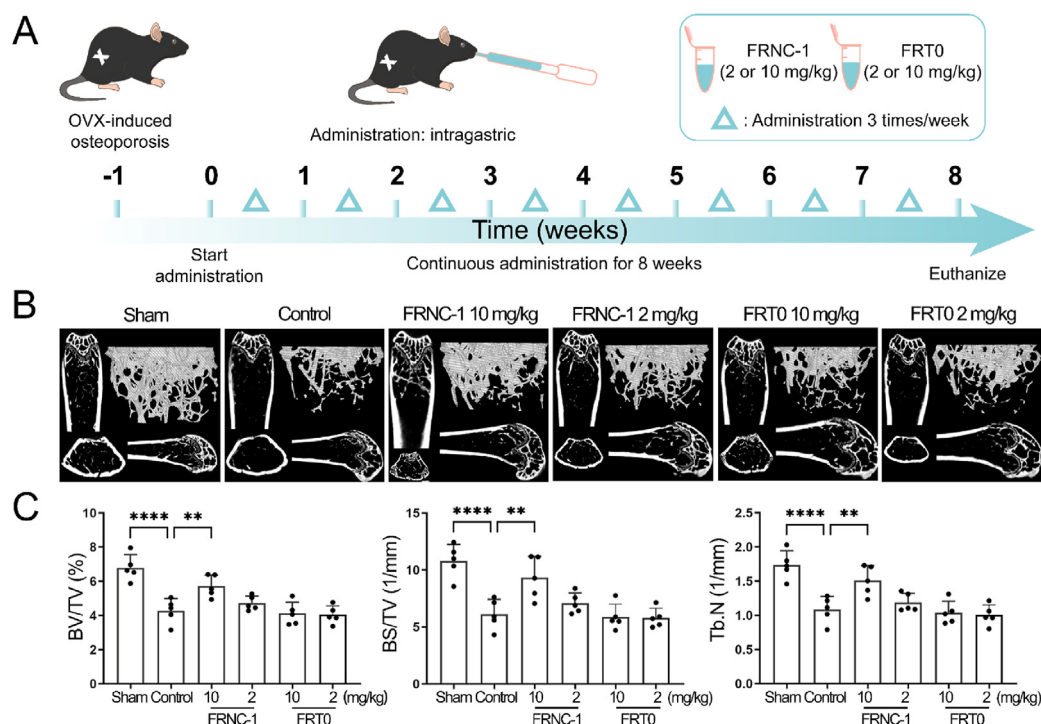
Figure 5 Oral administration of FRNC-1 effectively prevented OVX-induced bone loss *in vivo*. (A) The OVX mice experimental design and therapeutic scheme of FRNC-1. OVX mice were treated with FRNC-1 or FRT0 by oral administration according to the program: 3 doses of 2 or 10 mg/kg weekly for 56 days. (B) Each mouse's femurs were scanned using a high-resolution micro-CT, and the results were used to calculate microstructural indices. (C) Microstructural indicators including BV/TV, BS/TV and Tb.N were quantitively analyzed (**$P < 0.01$; ****$P < 0.0001$). Statistics were expressed as the means $\pm$ SD, $n = 5$.

peptide drug candidate to date for osteoporosis therapy. Our findings pave the way for the creation of stapled peptide-based therapeutics and open up the possibility to noninvasive and safe peptide administration. More investigation about pharmacological and pharmacokinetic profiles are in progress in our lab.

4. Experimental

4.1. Materials and animal experiments

The reagents involved in this article were provided by Titan Technology Co., Ltd. MBHA amide resin was provided by Tianjin Nankai Hecheng Technology Co., Ltd. C57BL/6J mice were provided by CAVENS Laboratories (Changzhou, China), and mouse experiments were approved by the Animal Care and Ethics Committee of the School of Life Sciences, Shanghai University (Shanghai, China) in accordance with the National Institutes of Health (NIH) Care and Use of Laboratory Animals Guide.

4.2. Synthesis of stapled peptides

The SPPS-assisted peptide sequence assembly was performed on a solid phase support of rink amide resin. The resin (333 mg, 0.1 mmol) was swelled by soaking in dichloromethane for 20 min. The Fmoc group was removed by incubating resin (333 mg, 0.1 mmol) in 20% piperidine in DMF for two 5 min. After that, the amino acid was coupled to the resin at 60 °C for 20 min using oxyma (5 equivalents), Fmoc-AA-OH (5 equivalents) and N,N'-

diisopropylcarbodiimide (10 equivalents) that dissolved in N-methylpyrrolidone (6 mL). Until amino acids all were coupled to the resin, the deprotection, washing and coupling was repeated. Two equivalents of the unnatural amino acid were used during the 2 h coupling of S_5. Next, the Ac reside was introduced to the resin using 6 mL pyridine and acetic anhydride ($v/v = 1:1$) at ambient temperature for 20 min. Two 2 h RCM reactions in 1,2-dichloroethane at ambient temperature were carried out using Grubbs' first-generation catalyst at a concentration of 10 mmol/L. Then, the resin was cleaved to release the crude stapled peptides using cocktail B (phenol:water:TFA:TIPS = 5:5:88:2, $v/v/v/v$) for 4 h. Cold diethyl ether was used to precipitate the peptides, followed by the purification through RP-HPLC. HPLC analysis confirmed that all purified peptides were more than 95% pure.

4.3. Preparative and analytical HPLC and mass spectrometry

Using preparative HPLC (SD-1 VARIAN) and a YMC-Pack ODS-AQ column (250 mm × 20 mm, I.D.S-5 μm, 12 nm), the desired peptides were purified with a flow rate of 15 mL/min monitored at 214 nm. The elution of each peptide was achieved by progressively enhancing the ratio of solution B (acetonitrile) to solution A (water). The solution A and B both contained 0.1% TFA. Using analytic RP-HPLC (Agilent Technologies 1260 Infinity) and an analytical column (type: Waters XBridge C18, 4.6 mm × 150 mm, 5 μm, flow rate: 1.0 mL/min, r.t.), the purified peptides were analyzed monitored at 241 nm. A linear gradient was lasted from 5 to 30 min with 5%−65% solution B. HR-Q-TOF-MS was

performed using an Agilent 6538 UHD Accurate Mass Q-TOF mass spectrometer.

4.4. CD spectroscopy

The stapled peptides were soluble in PB with a pH of 7.2 at the concentration of $10-50$ μmol/L. CD experiments were performed using a Jasco J-715 spectropolarimeter at ambient temperature. A quartz cuvette with 1 mm path length was used for the spectra collection (wavelength: $185-255$ nm; step resolution: 0.0001 μm; speed: 1.2 μm/h; accumulations: 6; bandwidth, 0.0001 μm. We calculated the helicity of each peptide using Eq. (1):

$$\alpha \text{ (Helicity)} = \frac{[\theta]_{222}}{[\theta]_{max}} \times 100\% = \frac{\theta_{222}/(10 \times c \times l)}{(-44000 + 250T) \times (1 - k/n)} \tag{1}$$

where $[\theta]_{222}/[\theta]_{max}$ is the helicity of peptide, $[\theta]_{222}$ is the calculated ellipticity at 222 nm (deg.cm^2/dmol), θ_{222} is the directly observed ellipticity (mdeg), c is the molar concentration of the peptide, l is the path length (cm), T is the temperature (25 °C), k stands for a fixed constant equaling to 4.0, and n stands for the number of amino acid residues in the peptide.

4.5. Protease stability

Chymotrypsin was dissolved at a concentration of 100 ng/L in 50 mmol/L PBS with a pH of 7.4 and 2 mmol/L CaCl$_2$. Using DMSO at 1 mmol/L, FRNC-1 and FRT0 were dissolved. At ambient temperature, the mixture was obtained by adding peptide to chymotrypsin solution. The mixture was monitored by analytical HPLC at 214 nm at various time points to determine the percentage of residual peptide.

4.6. Plasma stability

Human plasma and peptides were mixed and placed in an oven at 37 °C, and incubated for a predetermined time of 0, 0.08, 0.25, 0.5, 1, 2, 4, 6, 8, 12, 24, and 48 h. Each time, 50 μL mixture was taken, and 100 μL of ethanol termination solution was added. The supernatant after 10 min of centrifugation at 13,400 rpm was subjected to HPLC analysis.

4.7. Structural modeling analysis

Protein data bank provided the original, unmodified FRT0 peptide structures (PDB ID: 1GNG). Discovery Studio Visualizer was used to generate the expected model and the stapled structure of FRNC-1. FRNC-1 and phosphorylated GSK-3β interaction model was predicted using AutoDock (http://autodock.scripps.edu). Each structural diagrams were created and analyzed using PyMOL (https://pymol.org/2).

4.8. Cell culture

4.8.1. BMMs were derived from the bone marrow of female C57BL/6J mice aged 6 weeks
Flush mouse hindlimb bone marrow with α-MEM complete medium to obtain cells for isolation. Incubated at 37 °C with 5% CO$_2$, and cultured with medium supplemented with M-CSF (30 ng/mL). Cells could be used for subsequent experimental analysis when they occupied 90% of the area.

4.8.2. Mesenchymal stem cells (MSCs) were derived from the skulls of C57BL/6J neonatal mice
The skulls of C57BL/6J (CAVENS.LA, Guangzhou, China) neonatal mice were collected and washed with $10 \times$, $5 \times$, $1 \times$ penicillin−streptomycin and PBS. Incubated at 37 °C with 5% CO$_2$, cells were immersed in collagenase II (C8150; Solarbio, Beijing, China) and cultured overnight. Purified cells, obtained by washing with PBS and passing through a 70 μm mesh, were cultured in α-MEM, and the obtained MSCs were passaged and used for subsequent experiments.

4.9. Cytotoxicity assay

To confirm the cytotoxic impact of FRNC-1 on BMMs and MSCs, a CCK-8 test was conducted. 5×10^3 cells were cultured in 100 μL medium per well using the 96-well plates. After 24 h, FRT0 and FRNC-1 were added at a concentration gradient of 0.15625, 0.31, 0.62, 1.25, 5, 10 and 20 μmol/L, MSCs were incubated for 4 days, while BMMs were incubated for 2 or 7 days. CCK-8 reagent (#V31001; Beyotime Bio, Shanghai, China) was added to the plates (10 μL per well) for 1 h before the assay. The absorbance was measured with a Cytation 5 Imaging reader (Bio-Tek. Vermont, USA) at 450 nm.

4.10. Cellular permeability

In 96 wells of PE CellCarrier Ultra microplates, 5×10^3 BMMs were cultured per well. Induced media (10% FBS, 1% penicillin/streptomycin, a-MEM, 30 ng/mL M-CSF, and 50 ng/mL RANKL) or induced medium without RANKL was used to culture cells for 7 days. Nuclei was stained by Hoechst 33342 after 6 h treatment with 5 μmol/L FRNC-1. Photos were captured with a high-content analysis system.

4.11. Real-time quantitative PCR

In a 6-well plate, 2×10^5 BMMs were cultured per well. 24 h later, cells were cultured for 7 days using osteoclast induced medium with or without 1.25 or 2.5 μmol/L of FRT0 or FRNC-1. RNAiso Plus was used to extract total RNA. Reverse transcription of 1000 ng of extracted RNA to cDNA by Prime Script RT Master Mix. cDNA was blended with MonAmp™ SYBR®Green qPCR Mix and bidirectional primers and subjected to qPCR using qTOWER3. QPCR protocol according to the directions. The primers used for amplification were GAPDH (Forward: 5′-ACC CAG AAG ACT GTG GAT GG-3′, and Reverse: 5′-CAC ATT GGG GGT AGG AAC AC-3′); NFATc1 (Forward: 5′-GGG TCA GTG TGA CCG AAG AT-3′, and Reverse: 5′-GGA AGT CAG AAG TGG GTG GA-3′); CTSK (Forward: 5′-TCC GCA ATC CTT ACC GAA TA -3′, and Reverse: 5′-AAC TTG AAC ACC CAC ATC CTG-3′); TRAP (Forward: 5′-CCA TTG TTA GCC ACA TAC GG-3′, and Reverse: 5′-CAC TCA GCA CAT AGC CCA CA-3′); as well as MMP9 (Forward: 5′-CTG GAC AGC CAG ACA CTA AAG-3′, and Reverse: 5′-CTC GCG GCA AGT CTT CAG AG-3′). $2^{-\Delta\Delta CT}$ approach was used to normalize the data of GAPDH.

4.12. TRAP staining

From femoral and tibial bone marrow, primary BMMs were obtained and cultivated in induced medium. Then, a 96-well plate was inoculated with 8×10^3 BMMs per well, followed by the addition of FRT0 and FRNC-1 (0, 0.625, 1.25 and 2.5 μmol/L).

After maturing, osteoclasts were rinsed three times with PBS, fixed for 20 min using 4% paraformaldehyde, and TRAP stained. A Cytation 5 Imaging reader (Bio-Tek. Vermont, USA) was used to record these images.

4.13. Bone resorption assay

BMM cells were implanted into hydroxyapatite bone plates, 8×10^3 BMMs were cultured per well. Cells were grown for 7 days in induced medium with various concentrations of FRNC-1 and FRT0 (1.25 and 2.5 µmol/L). On the 8th day, the Cytation 5 Imaging reader was used to obtain photos of the reabsorption pits on the plate. (Bio-Tek. Vermont, USA). The percent resorption area per well and the quantitative results were based on analysis by ImageJ software.

4.14. F-actin staining

In a 96-well plate, 8×10^3 BMMs were cultured per well, growing in medium containing or without RANKL and various concentrations of FRNC-1 and FRT0 (1.25 and 2.5 µmol/L) for 7 days, with medium changes every 2 days. Fluorescence pictures were obtained using a Cytation 5 Imaging reader (Bio-Tek. Vermont, USA) after cells were dyed using Hoechst 33,342 and TRITC-labeled phalloidin (CA1610; Solarbio, Beijing, China) working solution.

4.15. ALP and alizarin red S staining

MSCs were grown in medium supplemented with L-ascorbic acid (50 µg/mL) and β-glycerophosphate (5 mmol/L) and or without 2.5 µmol/L FRNC-1 or FRT0. On the 8th day, ALP staining was conducted. The cells were rinsed three times for 10 min in PBS after being fixed with 4% PFA for 15 min. Then, an Alkaline Phosphatase Assay Kit (C3206; Biyotime, Jiangsu, China) was used for staining. Following 21 days, in a manner similar to ALP staining, cells were fixed. After that, the cells were successively rinsed three times for 10 min with PBS and 70% ethanol. Then, Alizarin Red S staining solution (G1452; Solarbio, Beijing, China) was applied, followed by washing with 50% ethanol and air drying. Using the Cytation™ 5, photographs were captured.

4.16. Western blot analysis

In a 6-well plate, 2×10^5 BMMs were cultured per well. The media was supplemented with various concentrations of FRT0/FRNC-1 (0, 10, 20, and 40 µmol/L), after 2 h, stimulated by adding RANKL to the media. After 0.5 h, the cells were lysed in RIPA solution containing PMSF. After centrifuged at $12,000 \times g$ for 15 min at 4 °C, the collected supernatants were combined with loading buffer, boiled for 10 min, and then collected. On 10% Bis-Tris acrylamide gels, the proteins were separated before being shifted over to PVDF membranes. 5% milk blocking membrane for 1 h before being treated 12 h at 4 °C with specific antibody. The membranes were rinsed with TBST and treated with secondary antibody for 1 h. The bands were observed with Bio-Rad ChemiDoc Imaging System.

4.17. Pull-Down assay

60 µL of Dynabeads™ M-280 Streptavidin was thrice washed using a binding buffer, and then mixed with 120 µL of 0.25 mg/mL FRNC-1 at room temperature and shaken for 30 min, subsequent to three rinses with binding buffer. Protein extraction was performed from BMMs, MCF7 and HCT116 cells using Western and IP lysates. The extracted proteins were incubated with Dynabeads for 2 h, washed with binding buffer followed by three washes with washing buffer and then three washes with binding buffer. The proteins linked to peptides were obtained by boiling in the lysate containing $5 \times$ loading buffer for Western blot.

4.18. In vivo experiments

4.18.1. OVX-induced osteoporosis model
C57BL/6J female mice from two groups were used for FRNC-1 subcutaneous injection and oral (intragastric) treatment.

The mice were bred in the Laboratory Animal Research Center, Institute of Translational Medicine, Shanghai University. The environment was set at 21–25 °C and 45%–65% moisture content, with a 12 h light/dark cycle, and the mice had full access to water and food. Some mice underwent bilateral oophorectomy under chloral hydrate anesthesia to induce osteoporosis. These osteoporosis model mice were separated into nondrug-treated (control) and drug-treated (FRNC-1/FRT0) groups. The rest of the animals, in which the ovaries were only exposed without surgical resection, were used as the sham group.

A total of 24 mice participated in subcutaneous injection treatment. The sham group had 8 mice, while the control group had 6, and 10 in the FRNC-1 groups: 2 and 5 mg/kg groups, 5 each. These mice were treated with FRNC-1 thrice weekly for a total of seven weeks. Similarly, the grouping of the 43 mice in the oral drug experiment was as follows: 8 mice in the control, 7 in the sham, 14 in the FRNC-1 groups (7 mice each in the 2 and 10 mg/kg groups), and 14 mice in the FRT0 treatment groups (7 mice each in the 2 and 10 mg/kg groups). Treatment was given 3 times each week for 56 days.

During the treatment period, the animals were weighed weekly. Fix the femurs in 4% PFA and euthanize all mice after 8 weeks. One side of the femur was used for micro-CT studies, the other side of the femur was used for non-demineralized bone sectioning.

4.18.2. Pharmacokinetics
The stock solution of FRNC-1 dissolved in methanol was added to serum at the final concentrations of 2000, 1000, 500, 250, 100, 25, 5, and 1 ng/mL for the establishment of a standard curve. FRNC-1 was delivered orally at 10 mg/kg and subcutaneously at 5 mg/kg to C57BL/6J mice. Whole blood was obtained from the orbital canthus vein of mice before and 30 min after administration of a drug. Whole blood was centrifuged with 3000 rpm for 15 min at 4 °C to obtain the supernatant (serum), and then 3 times the volume of methanol was added to precipitate proteins and other macromolecular substances in the serum. 4 °C centrifuge at 12,000 rpm for 10 min, and take the top layer of liquid for analysis. The concentration gradient of FRNC-1 and the supernatant was assessed by ultraperformance liquid chromatography-electrospray ionization-tandem triple quadrupole mass spectrometry (UPLCESL-QQQ-MS, Shimadzu 8040). XTIMATE C8 (2.1 mm × 100 mm, 3 µm, Welch, Shanghai, China) is equipped on the system. The column was 35 °C. Inject 10 µL. A gradient of 0.1% formic acid in water (buffer A) and 0.1% in acetonitrile (buffer B) eluted the analytes: 0.5–3.5 min 5%–95% B, 3.5–5.5 min 95% B, 5.5–5.6 min 95%–5% B, and 5.6–7.5 min 5% B. The areas

under the curve of the MS peaks (FRNC-1 [629.1858 m/z]) were integrated from base peak intensity chromatograms and plotted versus concentration to create standard curves. The standard curves: FRNC-1 ($y = 18.7682x + 68.1625$, $r^2 = 0.9996$, $r = 0.9998$). Based on the standard curve, the peak area of the same mass peaks was used to figure out how much peptide was in the supernatant.

4.19. Micro-CT scanning

Femur soaked in 4% PFA and evaluated using a high-resolution micro-CT scanner (SKYSCAN 1275; Bruker micro-CT, Kontich, Belgium). The scanning process with equidistant resolution of 9 μm with an X-ray energy of 50 kV and 60 μA. A number of detection indicators that can represent osteoporosis were used to measure the degree of osteoporosis. These included BV/TV, BS/TV, BMD, Tb.Th, Tb.N, and Tb. Sp.

4.20. Histological analysis

High-quality microscopes analyzed and photographed histological samples. Each sample counted osteoclasts per field.

4.21. H&E staining of visceral tissue

OVX mice were treated with FRNC-1 by subcutaneous injection with the schedule 3 weekly doses of 5 mg/kg administered for 7 weeks. Visceral tissue, including the heart, liver, spleen, lung and kidneys, was removed after the mice were euthanized and stored in 4% paraformaldehyde for 48 h. According to the tissue morphology, the target tissue was trimmed with a scalpel and placed in the embedding frame with numbered labels. The embedding frame containing the tissue was placed into the basket of the dehydrator, and gradually dehydrated with gradient alcohol and soak in wax inside the dehydrator. Melted wax was put into the embedded bottom mold. When the wax at the bottom of the mold to solidify slightly, the tissue was removed from the embedded frame carefully and placed into the embedded bottom mold with a completely flat state. The wax blocks that encapsulate the tissue were placed on a −20 °C freezer and completely solidified. The waxs were sliced into a paraffin pathological slicer with a thickness of 4 μm after pruning, then they were flatten it on a hot water spread at 42 °C. The tissues were lifted vertically with a glass slide and baked in a 60 °C baking machine for 30−60 min. According to the H&E staining manufacturer's instructions, tissues were stained. Photos were taken with a microscope.

Author contributions

Wei Cong, Huaxing Shen and Xiufei Liao contributed equally to this work. Wei Cong, Yulei Li, Honggang Hu and Xiang Li conceived the project and designed the experiments. The experiments were performed by Huaxing Shen, Xiufei Liao, Mengjun Zheng, Xianglong Kong, Zhe Wang and Si Chen. Wei Cong, Xuexiang Han, and Xiang Li wrote the manuscript. Xiang Li and Wei Cong designed and prepared the figures. All authors edited the manuscript and figures and approved the final version for submission.

Conflicts of interest

The authors have no conflicts of interest to declare.

Appendix A. Supporting information

Supporting data to this article can be found online at https://doi.org/10.1016/j.apsb.2023.05.004.

References

1. Khosla S, Hofbauer LC. Osteoporosis treatment: recent developments and ongoing challenges. *Lancet Diabetes Endocrinol* 2017;**5**:898−907.
2. Compston JE, McClung MR, Leslie WD. Osteoporosis. *Lancet* 2019;**393**:364−76.
3. Ensrud KE, Crandall CJ. Osteoporosis. *Ann Intern Med* 2017;**167**:ITC17−32.
4. Leder BZ, Tsai JN, Uihlein AV, Wallace PM, Lee H, Neer RM, et al. Denosumab and teriparatide transitions in postmenopausal osteoporosis (the DATA-Switch study): extension of a randomised controlled trial. *Lancet* 2015;**386**:1147−55.
5. Lufkin EG, Sarkar S, Kulkarni PM, Ciaccia AV, Siddhanti S, Stock J, et al. Antiresorptive treatment of postmenopausal osteoporosis: review of randomized clinical studies and rationale for the Evista alendronate comparison (EVA) trial. *Curr Med Res Opin* 2004;**20**:351−7.
6. Reid IR, Billington EO. Drug therapy for osteoporosis in older adults. *Lancet* 2022;**399**:1080−92.
7. Monroe DG, McGee-Lawrence ME, Oursler MJ, Westendorf JJ. Update on Wnt signaling in bone cell biology and bone disease. *Gene* 2012;**492**:1−18.
8. Wu M, Chen W, Lu Y, Zhu G, Hao L, Li YP. Galpha13 negatively controls osteoclastogenesis through inhibition of the Akt-GSK3beta-NFATc1 signalling pathway. *Nat Commun* 2017;**8**:13700.
9. Liu T, Cong W, Ye L, Xu X, Liao X, Xie G, et al. Rational design of stapled peptides targeting phosphorylated GSK3β for regulating osteoclast differentiation. *RSC Adv* 2020;**10**:7758−63.
10. Zhu Q, Chen Z, Paul PK, Lu Y, Wu W, Qi J. Oral delivery of proteins and peptides: challenges, status quo and future perspectives. *Acta Pharm Sin B* 2021;**11**:2416−48.
11. Philippe GJB, Craik DJ, Henriques ST. Converting peptides into drugs targeting intracellular protein−protein interactions. *Drug Discov Today* 2021;**26**:1521−31.
12. Wang L, Wang N, Zhang W, Cheng X, Yan Z, Shao G, et al. Therapeutic peptides: current applications and future directions. *Signal Transduct Targeted Ther* 2022;**7**:48.
13. Dubey SK, Parab S, Dabholkar N, Agrawal M, Singhvi G, Alexander A, et al. Oral peptide delivery: challenges and the way ahead. *Drug Discov Today* 2021;**26**:931−50.
14. Bucheit JD, Pamulapati LG, Carter N, Malloy K, Dixon DL, Sisson EM. Oral semaglutide: a review of the first oral glucagon-like peptide 1 receptor agonist. *Diabetes Technol Therapeut* 2020;**22**:10−8.
15. Zizzari AT, Pliatsika D, Gall FM, Fischer T, Riedl R. New perspectives in oral peptide delivery. *Drug Discov Today* 2021;**26**:1097−105.
16. Guarracino DA, Riordan JA, Barreto GM, Oldfield AL, Kouba CM, Agrinsoni D. Macrocyclic control in helix mimetics. *Chem Rev* 2019;**119**:9915−49.

17. Kurrikoff K, Aphkhazava D, Langel U. The future of peptides in cancer treatment. *Curr Opin Pharmacol* 2019;**47**:27−32.

18. Reguera L, Rivera DG. Multicomponent reaction toolbox for peptide macrocyclization and stapling. *Chem Rev* 2019;**119**:9836−60.

19. Yan S, Yan J, Liu D, Li X, Kang Q, You W, et al. A nano-predator of pathological MDMX construct by clearable supramolecular gold(I)-thiol-peptide complexes achieves safe and potent anti-tumor activity. *Theranostics* 2021;**11**:6833−46.

20. Li X, Chen S, Zhang WD, Hu HG. Stapled helical peptides bearing different anchoring residues. *Chem Rev* 2020;**120**:10079−144.

21. Li X, Tolbert WD, Hu HG, Gohain N, Zou Y, Niu F, et al. Dithiocarbamate-inspired side chain stapling chemistry for peptide drug design. *Chem Sci* 2019;**10**:1522−30.

22. Li X, Zou Y, Hu HG. Different stapling-based peptide drug design: mimicking α-helix as inhibitors of protein−protein interaction. *Chin Chem Lett* 2018;**29**:1088−92.

23. Wu Y, Li YH, Li X, Zou Y, Liao HL, Liu L, et al. A novel peptide stapling strategy enables the retention of ring-closing amino acid side chains for the Wnt/beta-catenin signalling pathway. *Chem Sci* 2017;**8**: 7368−73.

24. Wu Y, Zou Y, Sun L, Garzino-Demo A, Hu H, Zhang W, et al. Peptide stapling with the retention of double native side-chains. *Chin Chem Lett* 2021;**32**:4045−8.

25. Schafmeister Cep J, Verdine GL. An all-hydrocarbon cross-linking system for enhancing the helicity and metabolic stability of peptides. *J Am Chem Soc* 2000;**122**:5891−2.

26. Walensky LD, Bird GH. Hydrocarbon-stapled peptides: principles, practice, and progress. *J Med Chem* 2014;**57**:6275−88.

27. Lai Y, Fois G, Flores JR, Tuvim MJ, Zhou Q, Yang K, et al. Inhibition of calcium-triggered secretion by hydrocarbon-stapled peptides. *Nature* 2022;**603**:949−56.

28. Lau YH, de Andrade P, Wu Y, Spring DR. Peptide stapling techniques based on different macrocyclisation chemistries. *Chem Soc Rev* 2015;**44**:91−102.

29. Feng M, Jin JQ, Xia L, Xiao T, Mei S, Wang X, et al. Pharmacological inhibition of β-Catenin/BCL9 interaction overcomes resistance to immune checkpoint blockades by modulating Treg cells. *Sci Adv* 2019;**5**:eaau5240.

30. Mitra S, Montgomery JE, Kolar MJ, Li G, Jeong KJ, Peng B, et al. Stapled peptide inhibitors of RAB25 target context-specific phenotypes in cancer. *Nat Commun* 2017;**8**:660.

31. Zheng M, Wang R, Chen S, Zou Y, Yan L, Zhao L, et al. Design, synthesis and antifungal activity of stapled Aurein1.2 peptides. *Antibiotics* 2021;**10**:956.

32. Zheng M, Cong W, Peng H, Qing J, Shen H, Tang Y, et al. Stapled peptides targeting SARS-CoV-2 Spike protein HR1 inhibit the fusion of virus to its cell receptor. *J Med Chem* 2021;**64**:17486−95.

33. Liao H, Li X, Zhao L, Wang Y, Wang X, Wu Y, et al. A PROTAC peptide induces durable beta-catenin degradation and suppresses Wnt-dependent intestinal cancer. *Cell Discov* 2020;**6**:35.

34. Mourtada R, Herce HD, Yin DJ, Moroco JA, Wales TE, Engen JR, et al. Design of stapled antimicrobial peptides that are stable, nontoxic and kill antibiotic-resistant bacteria in mice. *Nat Biotechnol* 2019;**37**:1186−97.

35. Bird GH, Madani N, Perry AF, Princiotto AM, Supko JG, He X, et al. Hydrocarbon double-stapling remedies the proteolytic instability of a lengthy peptide therapeutic. *Proc Natl Acad Sci U S A* 2010;**107**: 14093−8.

36. Yost C, Ghr Farr, Pierce SB, Ferkey DM, Chen MM, Kimelman D. GBP, an inhibitor of GSK-3, is implicated in Xenopus development and oncogenesis. *Cell* 1998;**93**:1031−41.

37. Bax B, Carter PS, Lewis C, Guy AR, Bridges A, Tanner R, et al. The structure of phosphorylated GSK-3β complexed with a peptide, FRATtide, that inhibits β-Catenin phosphorylation. *Structure* 2001;**9**:1143−52.

38. Ye J, Jiang J, Zhou Z, Weng Z, Xu Y, Liu L, et al. Near-infrared light and upconversion nanoparticle defined nitric oxide-based osteoporosis targeting therapy. *ACS Nano* 2021;**15**:13692−702.

39. Jacome-Galarza CE, Percin GI, Muller JT, Mass E, Lazarov T, Eitler J, et al. Developmental origin, functional maintenance and genetic rescue of osteoclasts. *Nature* 2019;**568**:541−5.

40. Phillips C, Roberts LR, Schade M, Bazin R, Bent A, Davies NL, et al. Design and structure of stapled peptides binding to estrogen receptors. *J Am Chem Soc* 2011;**133**:9696−9.

41. Yu M, Pal S, Paterson CW, Li JY, Tyagi AM, Adams J, et al. Ovariectomy induces bone loss via microbial-dependent trafficking of intestinal TNF+ T cells and Th17 cells. *J Clin Invest* 2021;**131**:e143137.